Journal of the Mechanics and Physics of Solids 109 (2017) 288–306

Contents lists available at ScienceDirect

Journal of the Mechanics and Physics of Solids

journal homepage: www.elsevier.com/locate/jmps

Interfacial self-healing of nanocomposite hydrogels: Theory and experiment

Qiming Wang*, Zheming Gao, Kunhao Yu

Sonny Astani Department of Civil and Environmental Engineering, University of Southern California, Los Angeles, CA 90089, USA

ARTICLE INFO

Article history:
Received 20 April 2017
Revised 15 June 2017
Accepted 14 August 2017
Available online 4 September 2017

Keywords:
Self-healing polymer
Dynamic bond
Interfacial strength
Nanocomposite hydrogel

ABSTRACT

Polymers with dynamic bonds are able to self-heal their fractured interfaces and restore the mechanical strengths. It is largely elusive how to analytically model this self-healing behavior to construct the mechanistic relationship between the self-healing properties (e.g., healed interfacial strength and equilibrium healing time) and the material compositions and healing conditions. Here, we take a self-healable nanocomposite hydrogel as an example to illustrate an interfacial self-healing theory for hydrogels with dynamic bonds. In the theory, we consider the free polymer chains diffuse across the interface and reform crosslinks to bridge the interface. We analytically reveal that the healed strengths of nanocomposite hydrogels increase with the healing time in an error-function-like form. The equilibrium self-healing time of the full-strength recovery decreases with the temperature and increases with the nanoparticle concentration. We further analytically reveal that the healed interfacial strength decreases with increasing delaying time before the healing process. The theoretical results quantitatively match with our experiments on nanosilica hydrogels, and also agree well with other researchers' experiments on nanoclay hydrogels. We expect that this theory would open promising avenues for quantitative understanding of the self-healing mechanics of various polymers with dynamic bonds, and offer insights for designing high-performance self-healing polymers.

1. Introduction

To mimic human muscles and skins that can autonomously repair themselves, a number of synthetic self-healing polymers have been developed. These self-healing polymers generally fall into two categories. The first category is so called "extrinsic self-healing" which harnesses encapsulates of curing agents that can be released upon fracture or damage to rebridge the fractured interfaces or damaged areas (Blaiszik et al., 2010; Toohey et al., 2007; White et al., 2001). The second category is so called "intrinsic self-healing" which harnesses dynamic bonds that can autonomously reform after fracture or dissociation (Wojtecki et al., 2011). The dynamic bonds include dynamic covalent bonds (Chen et al., 2002; Ghosh and Urban, 2009; Skene and Lehn, 2004), hydrogen bonds (Chen et al., 2012; Cordier et al., 2008; Phadke et al., 2012; Sijbesma et al., 1997; Wang et al., 2013), metal-ligand coordination (Burnworth et al., 2011; Holten-Andersen et al., 2011; Nakahata et al., 2011), hydrophobic interactions (Gulyuz and Okay, 2014; Okay, 2015), and ionic interactions (Haraguchi et al., 2011; Mayumi et al., 2016; Sun et al., 2012; Sun et al., 2013; Wang et al., 2010). These self-healing polymers pose great potential for smart and adaptive materials that can repair fracture or damage at the molecular or micron scale, and restore their me-

* Corresponding author.
E-mail address: qimingw@usc.edu (Q. Wang).

http://dx.doi.org/10.1016/j.jmps.2017.08.004
0022-5096/

chanical strengths at the macroscopic scale, and thus can be potentially useful in a wide range of applications in automobile, aerospace and biomedical engineering.

Despite the prosperous studies on synthesizing self-healing polymers, mechanistic modeling of interfacial self-healing behaviors is still at the very beginning (Blaiszik et al., 2010; Burattini et al., 2010; Hui and Long, 2012; Long et al., 2014; Wojtecki et al., 2011; Wool, 2008; Wu et al., 2008; Yang and Urban, 2013). Although scaling analysis and computational models of self-healing behaviors of polymers have been proposed (Balazs, 2007; Ge et al., 2014; Stukalin et al., 2013; Wool and O'connor, 1981; Wool, 1995, 2008; Zhang and Rong, 2012), an analytical model to elucidate the relationship between the interfacial self-healing strength is still unavailable. Yu et al. reported an analytical theory to model the interfacial welding of a polymer under relatively high temperatures (Yu et al., 2016); the welding is different from interfacial self-healing in that self-healing behaviors usually occur at low temperatures. In addition, the self-healed polymers, supposed to be mechanically weaker than the virgin polymers, however, usually feature stress-strain curves that superpose the virgin ones and only break with lower strengths (Blaiszik et al., 2010; Burattini et al., 2010; Wojtecki et al., 2011; Wool, 2008; Wu et al., 2008; Yang and Urban, 2013). This confusion has not been explained by existing models.

Towards elucidating the self-healing mechanisms of polymers with dynamic bonds (the second type self-healing polymer), we here focus on a hydrogel that is composed of polymer networks crosslinked by inorganic nanoparticles through ionic bonds. The nanoparticles can be of wide varieties, ranging from nanoclay, silica, silsesquioxane, titania, graphene oxide to carbon nanotubes (Carlsson et al., 2010; Haraguchi, 2007, 2011a, b; Haraguchi et al., 2003; Haraguchi and Li, 2006; Haraguchi et al., 2007; Haraguchi and Li, 2005; Haraguchi and Song, 2007; Haraguchi and Takehisa, 2002; Haraguchi et al., 2002; Haraguchi et al., 2011; Huang et al., 2007; Ren et al., 2011; Wang et al., 2010). Unlike the usual organic crosslinkers that usually can only covalently attach less than 10 polymer chains around one crosslinker, the nanoparticle crosslinker with a large number of attaching sites on its surface is capable of attaching a large number of polymer chains (e.g., more than 100). In addition, different from the permanent covalent bonds, the bonding between the nanoparticles and the chains are through dynamic ionic-bonds (Carlsson et al., 2010; Haraguchi and Takehisa, 2002). Because of the dynamic bonding, the nanocomposite hydrogels are able to self-heal their strengths after fracture. However, how to analytically understand the interfacial self-healing behaviors under various healing conditions is still unclear (Haraguchi, 2011b; Haraguchi et al., 2011).

Here, we develop a polymer-network based theory to reveal the tensile strength of the self-healable nanocomposite hydrogels with various material compositions (particle concentration and chain length distribution) and under various healing conditions (healing time, healing temperatures and delaying time). The theory can explain the stress-strain behaviors of the nanocomposite hydrogels with self-healed interfaces. The theory enables us to understand the aforementioned stress-strain superposition puzzle (Blaiszik et al., 2010; Burattini et al., 2010; Wojtecki et al., 2011; Wool, 2008; Wu et al., 2008; Yang and Urban, 2013). The theory can also reveal that the strengths of the self-healed nanocomposite hydrogels increase with the healing time following an error-function-like shape. The healing time of full-strength recovery increases with decreasing healing temperature, increasing particle concentration and decreasing delaying time. The theoretical results are consistent with experiments on nanocomposite hydrogels with nanosilica or nanoclay crosslinkers.

The plan of the paper is as follows. Section 2 introduces the experimental procedures of the fabrication and self-healing testing of the nanocomposite hydrogels. Section 3 first presents an analytical theory to model the polymer networks of the original nanocomposite hydrogels and then presents a theory to explain the interfacial penetration of polymer chains and healing of polymer networks around the healing interface. Integrating two theories, we will construct a theoretical framework to explain the healing strengths of the nanocomposite hydrogels. Based on the theoretical framework, in Section 4 we analytically elucidate the stress-strain behaviors of self-healed nanocomposite hydrogels and their healing strengths in a function of the healing time. We then systematically examine the effects of chain length distribution, particle distance, Rouse friction coefficient, healing temperature, particle concentration and delaying time on the healing performance of the nanocomposite hydrogels. The theoretical results are quantitatively compared with experimentally measured results of nanocomposite hydrogels with nanosilica or nanoclay crosslinkers. The conclusive remarks will be given in Section 5.

2. Experimental

We choose a nanocomposite hydrogel with nanosilica crosslinkers as a representative self-healing polymer because the fabrication of this hydrogel is relatively easy. To synthesize the nanosilica hydrogel, we use potassium persulfate (KPS, Sigma-Aldrich) as the redox initiator and *N,N,N′,N′*-tetramethylethylenediamine (TEMED, Sigma-Aldrich) as the accelerator to induce the free-radical polymerization between the N,N-Dimethylacrylamide chains (DMA, Sigma-Aldrich) and the nanosilicas (TM-50, diameter ~9 nm, Sigma-Aldrich) at the room temperature (Rose et al., 2014). In a typical fabrication process, 7.699 g DI water and 5.712 g Ludox TM-50 (Sigma-Aldrich) in a plastic tube are mixed with Vortex for 30 min. Then, 1.485 g DMA, 0.0405 KPS and 22.5 μL TEMED are added into the plastic tube with additional mixing for 45 min (Carlsson et al., 2010). Finally, we transfer the hydrogel solution into a glass vial (length 36 mm, diameter 11 mm) for polymerization overnight. Once polymerized, the hydrogels are equilibrated at various temperatures (e.g., 316 K, 333 K, and 353 K) in a humid chamber. Experimental hydrogels are cut into two parts with a blade, after a period of delaying time ($t_d \geq 0$) brought into contact, and left in the humid chamber with a controlled temperature for varied healing time (Fig. 1a). Both original hydrogel samples and self-healed samples are mounted on a stress-strain tester (Model 5942, Instron), and uniaxially stretched with a low strain rate 0.06 s^{-1}. The experiment takes ~5 min, much smaller than the equilibrium healing time scale (hours). As shown in Fig. 1b, an original nanosilica hydrogel can be stretched to stretch ~28; once the interface is healed for 1.5 h at 333 K,

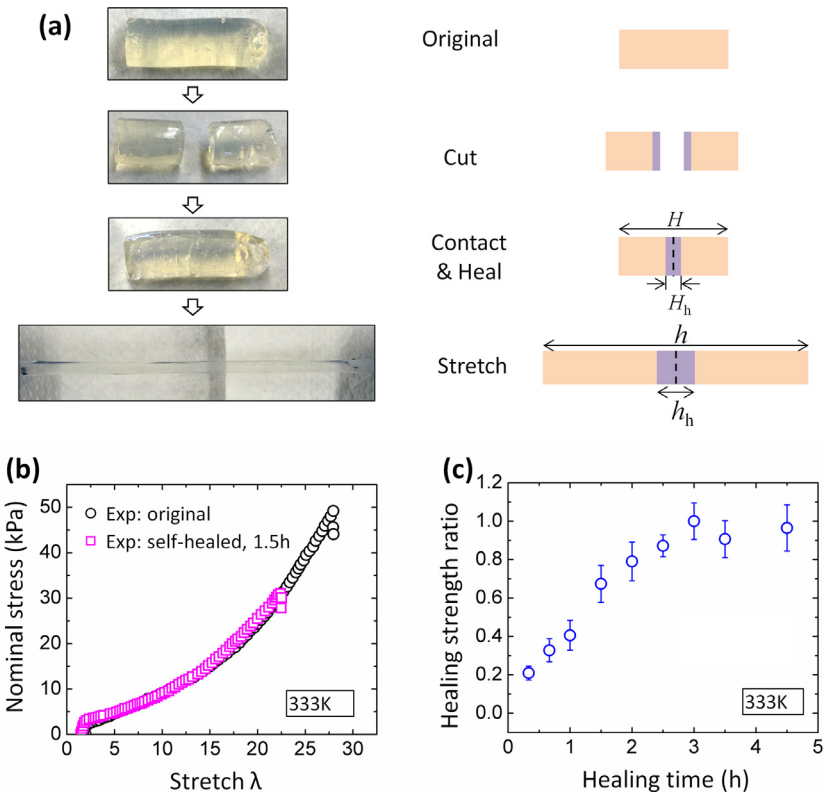

Fig. 1. (a) Experimental sequence and corresponding schematics of the self-healing process of a nanocomposite hydrogel: original nanocomposite hydrogel, cutting into two parts, bringing into contact and heal, and stretching the self-healed sample. (b) Representative experimentally measured stress-stretch behaviors of the original and the self-healed nanocomposite hydrogels. (c) Representative experimentally measured healing strength ratios in a function of healing time of the nanocomposite hydrogel.

the nanosilica hydrogel can be stretched to stretch ~22.5 with stress-stretch behavior almost superposing the original one. To quantify the healing performance, we denote a term called healing strength ratio as the ratio between the maximum nominal stress of the healed hydrogel and that of the original hydrogel. We further perform the healing tests for varied healing time from 5 min to 4.5 h, and plot the healing strength ratio in a function of healing time shown in Fig. 1c. The healing strength ratio first increases with increasing healing time until ~3–3.5 h, after which the healing strength ratio reaches a plateau of full recovery (within 90%–100%).

3. The theoretical model

The goal of this paper is to understand the interfacial self-healing strength and equilibrium healing time in relationships with the healing conditions and material compositions of the nanocomposite hydrogels. We start from the constitutive behaviors of the original nanocomposite hydrogels and depict the mechanism of their tensile strength. Then, we consider the healing process of two fractured hydrogel parts.

3.1. Tensile strength of original nanocomposite hydrogel

The nanocomposite hydrogels are synthesized through a free-radical polymerization between the polymer chains and nanoparticles, initiated by redox initiators. The anionic groups of the polymer chains can be ionically bonded to SO_3^- and K^+ groups which come from the redox initiators and are attached to the nanoparticle surface (Haraguchi and Takehisa, 2002). The nanoparticles, hooked by the polymer chains, in turn, are self-assembled into a three-dimensional architecture with a particle spacing (Williams et al., 2015).

To model the polymer network of the nanocomposite hydrogel, we consider the nanoparticles as crosslinkers to bridge a number of polymer chains that follow an inhomogeneous chain length distribution (Wang and Gao, 2016). The model is modified based on our recently reported constitutive model in the reference (Wang and Gao, 2016) with a simplified chain length distribution function (Wang et al., 2015).

Following the essential idea of polymer-network theories (Erman and Mark, 1997; Rubinstein and Colby, 2003; Treloar, 1975), we assume the polymer network of the nanoparticle hydrogel is constructed by layering unit cubes to span over the

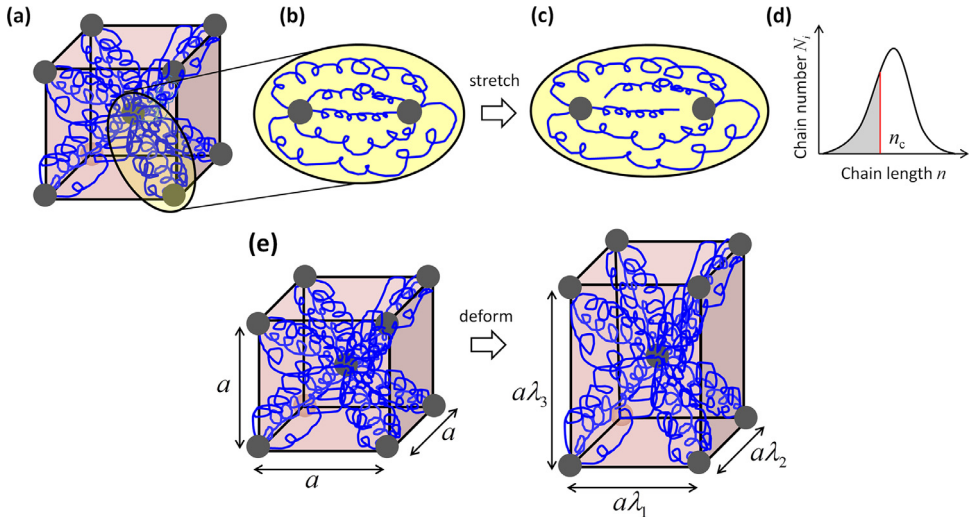

Fig. 2. (a) A body-centered network model. (b) The chain length is imhomogeneous between a particle pair. (c) Under stretch, short chains may be first detached from particles. (d) A representative chain length distribution. (e) Under macroscopic deformation (λ_1, λ_2, λ_3), the polymer network deforms following an affined deformation.

whole volume (unit cube shown in Fig. 2a). In each unit cube, nanoparticles are located at the corners and centers in a body-centered fashion (Fig. 2a). The corner and center particles form a particle pair, and polymer chains with inhomogeneous lengths attach between the particle pair (Fig. 2b). Under deformation, short polymer chains may be first detached from the particles (Fig. 2c). We consider that the ionic bonding strength is much smaller than the fracture strength of the covalent bonds within the chain (Wang and Gao, 2016); therefore, chain detachment rather than the chain fracture is considered in this model (Haraguchi, 2011b; Haraguchi and Takehisa, 2002).

Between two particles in a particle pair, we assume that N polymer chains are attached (Fig. 2b), each polymer chain made of freely-jointed Kuhn segments with each segment length b (Erman and Mark, 1997; Rubinstein and Colby, 2003; Treloar, 1975). We assume that the polymer chains can be classified into m types, each with the same Kuhn number. We denote the Kuhn number (chain length) of the ith type polymer chain as n_i, and the number of ith type chains as N_i, where $1 \le i \le m$ and $n_1 \le n_2 \le ...n_i... \le n_m$. The ith chain number follows a statistical distribution written as (Fig. 2d)

$$P_i(n_i) = \frac{N_i}{\sum_{i=1}^{m} N_i} = \frac{N_i}{N} \tag{1}$$

where $N = \sum_{i=1}^{m} N_i$ is the total chain number. Although the distribution can be formulated following Gaussian statistics (Bueche, 1960; Govindjee and Simo, 1991; Wang and Gao, 2016), for simplicity, we here consider a similar but simpler log-normal distribution function as (Wang et al., 2015)

$$P_i(n_i) = \frac{1}{n_i \delta \sqrt{2\pi}} \exp\left[-\frac{(\ln n_i - \psi)^2}{2\delta^2}\right] \tag{2}$$

where ψ and δ are the mean and standard deviation of $\ln n_i$, respectively. ψ denotes logarithm of the average chain length, and δ indicates the chain distribution width.

In the freely-joint state, the average end-to-end distance of the ith chain is

$$r_i^0 = \sqrt{n_i} b \tag{3}$$

Under deformation, the end-to-end distance of the ith chain becomes r_i, and the stretch of the ith chain can be expressed as

$$\Lambda_i = \frac{r_i}{r_i^0} \tag{4}$$

Considering the small particle size, we approximate the end-to-end distance of ith chain at the fabricated state as the particle distance L. At the deformed state, the hydrogel is under three principal stretch λ_1, λ_2, and λ_3. We assume that the deformation of the body-centered cube follows the affined deformation assumption (Arruda and Boyce, 1993; Rubinstein and Colby, 2003; Treloar, 1975), and is thus also deformed by λ_1, λ_2, and λ_3 (Fig. 2e). Therefore, the distance of the particle

pair at the deformed state becomes

$$r_i = L\sqrt{\frac{I_1}{3}} \tag{5}$$

where $I_1 = \lambda_1^2 + \lambda_2^2 + \lambda_3^2$ is the strain invariant. The stretch of the ith chain can be written as

$$\Lambda_i = \frac{r_i}{\sqrt{n_i}b} = \sqrt{\frac{I_1}{3}}\frac{L}{\sqrt{n_i}b} \tag{6}$$

The chain force on the ith chain at the current state is

$$f_i = \frac{k_B T}{b}\Gamma^{-1}\left(\frac{r_i}{n_i b}\right) = \frac{k_B T}{b}\Gamma^{-1}\left(\sqrt{\frac{I_1}{3}}\frac{L}{n_i b}\right) \tag{7}$$

where $\Gamma^{-1}()$ is the inverse Langevin function, and the Langevin function can be written as $\Gamma(x) = \coth x - 1/x$. k_B is Boltzmann constant and T is the absolute temperature in Kelvin. If the chain force is larger than the maximum chain-particle bonding strength f_{str}, the chain is detached from the particle. As shown in Eq. (7), short chains have a higher chain force. Therefore, at a certain deformation state, the short chains will be detached, leaving only long chains ($n > n_c$) attaching between the particle pair. The critical chain length can be calculated as

$$n_c = \frac{1}{\Gamma\left(\frac{f_{str}b}{k_B T}\right)}\frac{L}{b}\sqrt{\frac{I_1}{3}} \tag{8}$$

where $n_c > n_1$ and n_c is the chain length of the cth type of chain ($c \geq 1$). As the strain in the hydrogel increases, the critical chain length n_c becomes larger (c larger), leaving less long chains attaching between particles (Fig. 2d).

The free energy of deforming the hydrogel network comes from deforming all polymer chains between the particle pairs, and mixing between polymer network and water (Flory, 1953; Flory and Rehner Jr, 1943; Hong et al., 2008). The free energy can be written as

$$W = W_s + W_m \tag{9}$$

where W_s is the strain energy of the polymer network and W_m is the mixing free energy. Here we assume W_m remains constant, because the water diffusion time scale (~30 min) is much larger than the experimental testing time scale (~3 min) (Wang and Gao, 2016). Since the particle volume fraction is very small, we neglect the effect of nanoparticles on the overall free energy. As shown in Fig. 2a, the particles occupied by a cubic unit include the center particle plus 1/8 of 8 corner particles; therefore, the particle number in a unit should be 2. At the same time, the cubic unit includes 8 particle pairs. For a fabricated hydrogel, we assume the particle concentration (particle number per unit volume) as η_p, and the particle pair number per unit volume is $4\eta_p$ (Fig. 2a). Therefore, the free energy density of stretching the polymer network of the deformed original-hydrogel can be expressed as

$$W_s = 4\eta_p \sum_{i=c}^{m} (\omega_i N_i) \tag{10}$$

where the free energy of the deformed ith chain can be expressed as a function of strain invariant I_1 as (Kuhn and Grün, 1942)

$$\omega_i(I_1) = n_i k_B T\left[\frac{\beta_i}{\tanh\beta_i} + \ln\left(\frac{\beta_i}{\sinh\beta_i}\right)\right] \tag{11}$$

where $\beta_i = \Gamma^{-1}(\Lambda_i/\sqrt{n_i}) = \Gamma^{-1}(\sqrt{I_1/3}L/(n_i b))$. Eq. (10) only includes the contribution from the attached polymer chains (n_c to n_m).

We assume that the hydrogel is incompressible; therefore, we can write the principal stresses as

$$\sigma_1 = \lambda_1\frac{\partial W_s}{\partial \lambda_1} - \Pi \tag{12a}$$

$$\sigma_2 = \lambda_2\frac{\partial W_s}{\partial \lambda_2} - \Pi \tag{12b}$$

$$\sigma_3 = \lambda_3\frac{\partial W_s}{\partial \lambda_3} - \Pi \tag{12c}$$

where Π is the hydrostatic pressure to enforce the incompressibility. When the hydrogel is under a uniaxial tension with stretch $\lambda_1 = \lambda$ and $\lambda_2 = \lambda_3 = \lambda^{-1/2}$, the Cauchy stress along the stretching direction can be calculated as

$$\sigma_1 = 4\eta_p k_B T\frac{L}{b}\left(\lambda^2 - \lambda^{-1}\right)\sum_{i=c}^{m}\left(\frac{N_i\beta_i}{\sqrt{3I_1}}\right) \tag{13}$$

where $I_1 = \lambda^2 + 2\lambda^{-1}$and $\beta_i = \Gamma^{-1}(L/(n_i b)\sqrt{I_1/3})$. The nominal stress along the stretching direction is thus written as

$$s_1 = 4\eta_p k_B T \frac{L}{b}\left(\lambda - \lambda^2\right)\sum_{i=c}^{m}\left(\frac{N_i\beta_i}{\sqrt{3I_1}}\right) \tag{14}$$

When the applied strains are small, the nominal stresses in the hydrogel increase as the strains increase. However, as the applied strains become large enough, the portion of the attached chains between the particle pairs become less and less (c is larger, Fig. 2d), and the stresses in the hydrogel may decrease with increasing strains when most of the polymer chains are detached from particles. Therefore, it is expected that the nominal stresses in the hydrogel should first increase and then decrease with increasing strains, with a peak point in the middle. In the strain-controlled tensile testing experiment, the peak point is corresponding to a breaking of the nanocomposite hydrogels into two parts, and the corresponding stress is the hydrogel tensile strength.

3.2. Interfacial self-healing process of nanocomposite hydrogels

Next, we consider the interfacial self-healing of the nanocomposite hydrogels. We here take a simple experimental geometry (i.e., a hydrogel rod/bar) to construct the analytical model, and the model can be easily extended to other specimen geometries. As shown in Fig. 1a, a cylindrical nanocomposite gel bar is first cut into two parts in the middle with a blade. Immediately after the cutting, the two pieces are brought into contact for a period of healing time t at temperature T. After the healing process, the sample is uniaxially stretched until fractured in the middle (at the self-healing interface). The measured maximum stress is treated as the healed strength of the hydrogel. We here separate the self-healing process into multiple steps and consider each step as follows.

3.2.1. Cutting process

In the cutting process (Fig. 3ab), we use a sharp blade to cut through the hydrogel bar. For simplicity of analysis, we assume the cutting position is located in the middle of polymer chains between particle pairs as shown in Fig. 3ab. At the cutting tip, the blade highly deforms the polymer chains until the chains are detached from the particles. Since the chain strength is much larger than the chain-particle bonding strength, we assume that the polymer chains can only be detached from the particle surfaces without breaking in the middle of the chains (Wang and Gao, 2016). At the detachment point, the chain may be detached from either particle, with the other end being still attached on the other particle. We assume that each particle of a particle-pair still attaches half portion of polymer chains after cutting (Fig. 3b).

As shown in Fig. 3b, we denote two parts of the initial unit cube as A and B, respectively. Right after the cutting (Fig. 3b), the polymer chains detached from particles in hydrogel piece B are stretched out of the B hydrogel piece, and their end groups are dropped onto the surface of hydrogel piece A. To keep the story simple, we here first consider that the two hydrogel pieces are brought into contact immediately after cutting, and therefore the end groups of the hydrogel chains are still located on the cutting surfaces, without enough time to reorganize within the hydrogel piece A. We will further consider the effect of delaying time in Section 4.7.

3.2.2. Inter-diffusion process

When cutting-separated two parts are brought into contact, the chains with one end attached to one nanoparticle and the other end freely diffuse across the interface to find nanoparticles in the other piece of the hydrogel. From a thermodynamics perspective, the molecular configuration at the fabricated state should be the most stable state under the given material composition. When the cutting-separated two parts are brought into contact, the most likely trend is to return to the initial stable configuration. Therefore, we here assume the polymer chains only diffuse to the opposite side of the interface but do not loop back to their own side. Similar arguments can be found in modeling chain motions at polymer melt interfaces (Kim et al., 1996; Kim and Wool, 1983).

As shown in Fig. 3b, the free chains on one particle (denoted as I) are expected to presumably diffuse in any angles across the interface. However, due to the electrostatic attraction between the free end group and the redox initiators on the particle surfaces, the polymer chains are assumed to target to only four particles (denoted as II-V) in a self-assembly fashion, forming four particle-particle pairs (Haraguchi and Takehisa, 2002; Williams et al., 2015). Since the behaviors between each particle pair should be similar, we here only focus on one particle pair shown in Fig. 3c-f and consider a 1D-like problem between one particle-pair.

During the contact-healing process, the polymer chains with free ends are expected to diffuse across the interface to meet the other nanoparticle (Fig. 3d–f). Here, we follow de Gennes' reptation concept to consider that the polymer chain diffuses along a tube of its contour analogous to the motion of a snake (Fig. 3g) (De Gennes, 1979; de Gennes, 1971; Doi and Edwards, 1978; Rubinstein and Colby, 2003). The chain diffuses out of the tube with a segment called "minor chain" (Kim and Wool, 1983; Whitlow and Wool, 1991; Zhang and Wool, 1989). The curvilinear motion of the polymer chain is characterized by the Rouse friction model with the curvilinear diffusion coefficient D_c written as (De Gennes, 1979; Rouse Jr, 1953; Rubinstein and Colby, 2003)

$$D_c = \frac{k_B T}{n_i \xi} \tag{15}$$

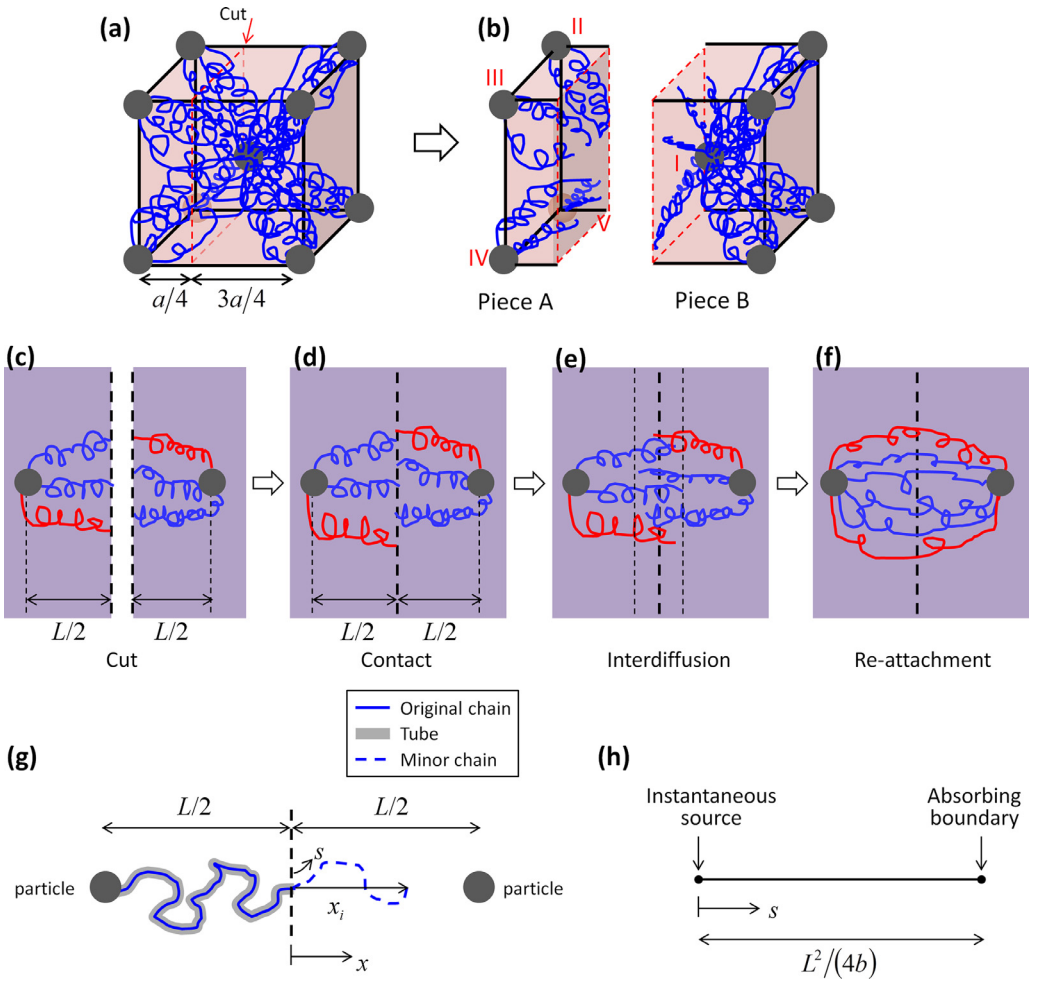

Fig. 3. (a, b) Schematics of the body-centered network model before and after the cutting process. The cutting is assumed to be located in the middle of two particles. (c–f) The schematics to show the self-healing process between a particle pair: (c) cutting in the middle, (d) two parts contact, (e) polymer chains inter-diffuse into respective hydrogel matrix, and (f) polymer chains with free end groups re-attach on the particle surfaces. The schematics for polymer chains in (c–f) only indicate the reorganization of chain conformations, but do not indicate polymer chain stretching during the healing process. (g) A schematic to show the diffusion behavior of a polymer chain between a particle pair. (h) An equivalent diffusion model between an instantaneous source on the contact interface and the absorbing boundary around the particle surface.

where n_i is the Kuhn segment number of the ith chain and ξ is the Rouse friction coefficient per Kuhn segment. As shown in Fig. 3g, we construct two coordinate systems s and x to indicate the curvilinear path of the minor chain and the direction along two particles, respectively. If the contour length of the ith minor chain is s_i, the corresponding end-to-end distance is x_i. We assume that the path selection of the minor chain follows Gaussian statistics (Kim and Wool, 1983; Whitlow and Wool, 1991; Zhang and Wool, 1989); therefore, the end-to-end distance and contour length can be related as (Rubinstein and Colby, 2003)

$$x_i \approx \sqrt{\frac{s_i}{b}}b = \sqrt{s_i b} \tag{16}$$

Therefore, the chain inter-diffusion between $x = 0$ and $x = L/2$ can be understood as the chain diffusion between $s = 0$ and x_i (Fig. 3h).

Along the curvilinear coordinate s, we can model the diffusion of the end group of the ith chain following a diffusion equation as (Fig. 3h) (Crank, 1979; Rubinstein and Colby, 2003)

$$\frac{\partial c_i^U(t,s)}{\partial t} = D_c \frac{\partial^2 c_i^U(t,s)}{\partial s^2} \tag{17}$$

where $c_i^U(t,s)$ is the number of the ith chain end groups per unit distance along s coordinate, and superscript letter "U" denotes the unattached chains. It is noted that the current chain diffusion model is different from the reptation model

which involves the chain entanglement effect (De Gennes, 1979; de Gennes, 1971; Doi and Edwards, 1978; Rubinstein and Colby, 2003). Here we use a curvilinear diffusion model to avoid the chain entanglement effect.

The initial condition of the diffusion behavior (Eq. (17)) is an instantaneous source at $s=0$, written as

$$c_i^U(t=0,s)=N_i\delta(s) \tag{18}$$

where $\delta(s)$ is a delta function with $\int_{-\infty}^{\infty}\delta(s)ds=1$. At $s=L^2/(4b)$, the boundary condition of the diffusion behavior is governed by the interaction behaviors between the chain end groups and the nanoparticles. More about chain-particle interactions at $s=L^2/(4b)$ will be discussed in Section 3.2.3.

3.2.3. Interaction kinetics between the polymer chain and the nanoparticle

The interaction between the chain end groups and the nanoparticles are governed by ionic interactions (Haraguchi and Takehisa, 2002). The chain-particle attaching and detaching behaviors follow a chemical kinetics (Bell, 1978; Wang et al., 2015). We assume the attaching reaction rate is k_f and the detaching reaction rate is k_r. The kinetics can be written as (Chapman et al., 1998; Morton, 2012)

$$\frac{dc_i^A}{dt}=k_fc_i^U-k_rc_i^A \tag{19}$$

where c_i^A is the number density of the attached ith chains and c_i^U is the number density of the unattached ith chains around the particle (at $s=L^2/(4b)$). To model the ionic reaction induced attaching or bonding here, we consider the ionic bonding only takes one step, and thus only consider the first reaction order. Similar models of first-order ionic reactions have been widely adopted to model ionic polymerization or binding (Chapman et al., 1998; Morton, 2012). Since the attaching behavior is governed by the attractive ionic interaction between the chain end groups and the nanoparticle, the attaching reaction rate k_f is assumed to be much larger than the detaching reaction rate k_r (Bell, 1978). Eq. (19) can thus be reduced as

$$\frac{dc_i^A}{dt}=k_fc_i^U \tag{20}$$

We further assume that the time scale of the ionic bonding that governed by $1/k_f$ is from seconds to minutes much smaller than the time scale of diffusion hours (Bell, 1978; Haraguchi et al., 2011; Ribas-Arino and Marx, 2012). Therefore, the chain-nanoparticle behavior can be understood as follows: whenever a chain end group diffuses to position $x=L/2$ (i.e., $s=L^2/(4b)$), it is quickly absorbed on the nanoparticle. The unattached chain end group concentration thus always vanishes at$s=L^2/(4b)$, following an absorbing boundary condition written as (Fig. 3h)

$$c_i^U\left(t,s=L^2/(4b)\right)\approx 0 \tag{21}$$

The absorbing boundary condition Eq. (21) promotes the diffusion of the polymer chain ends towards the particle surfaces.

It is noted that to simplify the problem and focus on the essential physics, we made two assumptions here: the attaching reaction rate is larger than the detaching reaction rate, and the ionic reaction time scale is much smaller than the diffusion time scale. It is only valid for relatively strong ionic interaction between the chain end groups and redox ions on nanoparticles. If the attaching reaction rate is in a similar order of magnitude as that of the detaching reaction rate, or the time scale of the ionic reaction is comparable with that of the diffusion process, a reaction time scale should be introduced in the problem (Hui and Long, 2012; Long et al., 2014).

3.2.4. Behaviors of self-healed sample

We then understand the mechanical behaviors of the self-healed hydrogel samples. When two hydrogel parts are brought into contact to heal the interface, the length of the healed sample is H and the length of the healed sample under stretching is h (Fig. 1a). Around the self-healing interface, polymer chains interpenetrate into each other, forming a self-healed region shown as the purple region in Fig. 1a. We denote the length of the self-healed region as H_h, and this region elongates to h_h under uniaxial stretching. The stretch of the self-healed region is

$$\lambda_h=\frac{h_h}{H_h} \tag{22}$$

Here, the self-healed hydrogel can be treated as a composite with original hydrogel regions and self-healed regions connected in a series. The stretch of the original hydrogel region is

$$\lambda=\frac{h-h_s}{H-H_s} \tag{23}$$

Since the healing region is so small, i.e., $h\gg h_s$ and $H\gg H_s$, the stretch of the self-healed hydrogel sample can be estimated as

$$\frac{h}{H}\approx\frac{h-h_s}{H-H_s}=\lambda \tag{24}$$

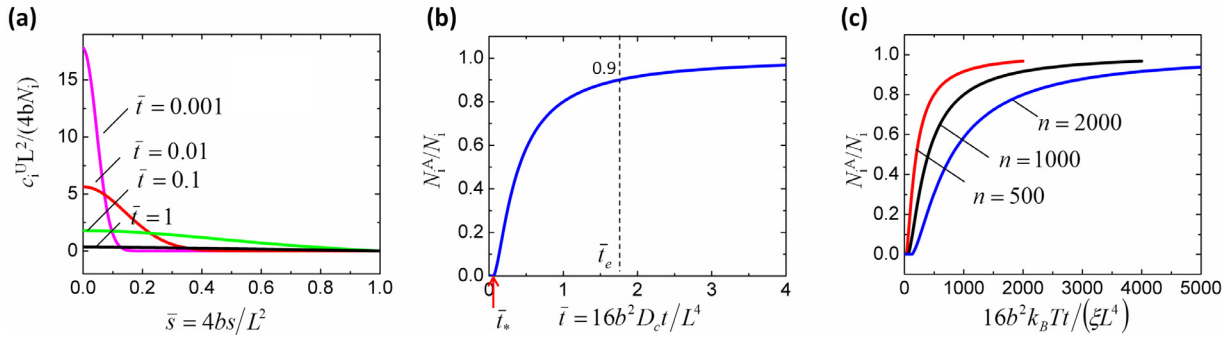

Fig. 4. (a) Unattached *i*th polymer chains distributed along the curvilinear coordinate between a particle pair. (b) Attached *i*th polymer chains in a function of normalized diffusion time. (c) Attached *i*th polymer chains in functions of diffusion time for various chain lengths.

In the stretched self-healed region, the number of *i*th chain between a particle pair is N_i^A $(c \le i \le m)$, which can be calculated following Sections 3.2.2–3.2.3 as

$$\frac{N_i^A}{N_i} = 1 - \int_0^{L^2/4b} \frac{c_i^U(s,t)}{N_i} ds \tag{25}$$

where $c_i^U(s,t)$ can be obtained by solving the diffusion equation shown in Eq. (17) with the initial and boundary conditions shown in Eqs. (18) and (21), written as

$$c_i^U(s,t) = \frac{2N_i}{\sqrt{4\pi D_c t}}\left[\exp\left(-\frac{s^2}{4D_c t}\right) - \exp\left(-\frac{\left(s-L^2/2b\right)^2}{4D_c t}\right)\right] \tag{26}$$

where $0 \le s \le L^2/(4b)$.

The stretching free energy density of this self-healed region can be expressed as

$$W_{sh} = 4\eta_p \sum_{i=c}^{m} \left[\omega_i(I_{1h}) N_i^A\right] \tag{27}$$

where $\omega_i(I_{1h})$ can be expressed as $\omega_i(I_{1h}) = n_i k_B T[\frac{\beta_{ih}}{\tanh\beta_{ih}} + \ln(\frac{\beta_{ih}}{\sinh\beta_{ih}})]$, $\beta_{ih} = \Gamma^{-1}(\sqrt{I_{1h}/3}L/(n_i b))$ and $I_{1h} = \lambda_{1h}^2 + \lambda_{2h}^2 + \lambda_{3h}^2$. It is noted that N_i^A s a self-healing-time dependent function and W_{sh} is thus a self-healing-time-dependent function. The nominal stress along the stretching direction can be calculated as

$$s_{1h} = 4\eta_p k_B T \frac{L}{b}\left(\lambda_h - \lambda_h^2\right) \sum_{i=c}^{m} \left(\frac{N_i^A \beta_{ih}}{\sqrt{3I_{1h}}}\right) \tag{28}$$

where $I_{1h} = \lambda_h^2 + 2\lambda_h^{-1}$.

We assume that the initial cross-sections of original region and self-healed region are the same; therefore, the nominal stresses of the original hydrogel region and the self-healed region should be equal, i.e.

$$s_1(\lambda) = s_{1h}(\lambda_h) \tag{29}$$

where $s_1(\lambda)$ is the nominal stress in the original hydrogel region expressed as Eq. (14), and $s_{1h}(\lambda_h)$ is the nominal stress in the self-healed region expressed as Eq. (28).

4. Results

In this section, we will first present results of the inter-penetration behaviors of the polymer chains, and then the self-healing behaviors of the nanocomposite hydrogels. We will further discuss the effects of various model parameters, including chain length distribution, Rouse friction coefficient, and particle distance. We will compare the theoretical results with the experimentally measured results. Various experimental results will be presented to demonstrate the effects of healing temperature, particle concentration and delaying time on the self-healing behaviors.

4.1. Inter-diffusion behaviors

Fig. 4a presents the distribution of the normalized chain number density of the unattached *i*th chains $(c_i^U L^2/4b)/N_i$ along the normalized curvilinear coordinate $\bar{s} = s/(L^2/4b)$ at various normalized diffusion time $\bar{t} = D_c t/(L^4/16b^2)$ (see Eq. (26)). Due to the absorption boundary condition around the particle, with increasing diffusion time the free ends between $s = 0$

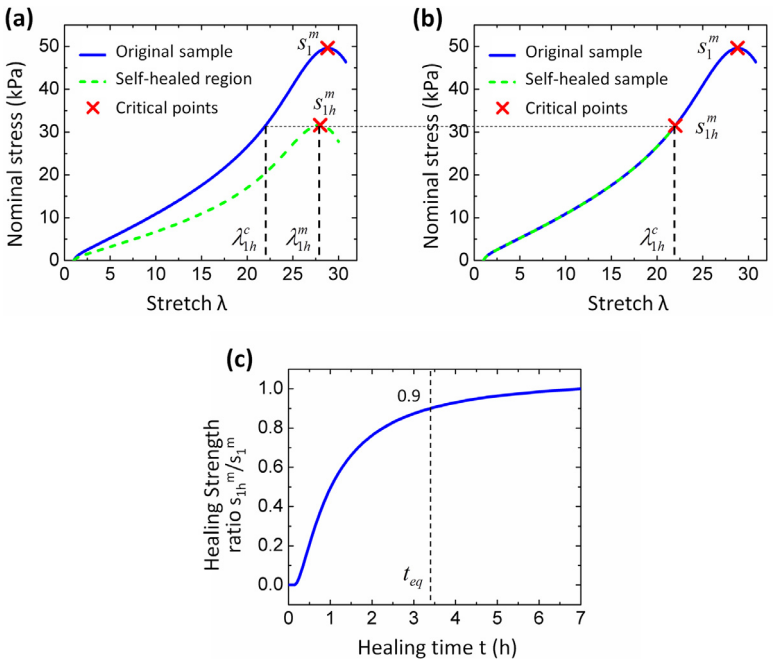

Fig. 5. (a) Theoretical stress-stretch behaviors of the original nanocomposite hydrogel and the self-healed nanocomposite hydrogel region. (b) Theoretical stress-stretch behaviors of the original and the self-healed nanocomposite hydrogel samples. (c) Theoretical healing strength ratio in a function of healing time. The following parameters are used to plot these curves: $L/b = 85$, $\psi = \ln[L^2/(4b^2)]$, $\delta = 0.12$, $\xi = 2.5 \times 10^{-8}$N/m, and $\eta_p = 8.2 \times 10^{19}$m^{-3}.

and $s = L^2/4b$ become less and less. In turn, the absorbed polymer chain (attached chain) number becomes larger and larger until a plateau (Fig. 4b, Eq. (25)). As shown in Fig. 4b, when the normalized diffusion time is smaller than $\bar{t}_* \approx 0.068$, no ith chain free ends arrive at the particle and the attached ith chain number is 0. After $\bar{t}_*$, the attached ith chain increases monotonically until reaching a plateau around $N_i^A \approx N_i$. From Fig. 4b, we can estimate normalized equilibrium diffusion time $\bar{t}_e$ when $N_i^A/N_i \approx 0.9$as $\bar{t}_e \approx 1.75$ (corresponding equilibrium diffusion time $t_e = \bar{t}_e(L^4/16b^2)/D_c$). Since the curvilinear diffusivity D_c is larger for shorter chain length n_i (Eq. (15)), the equilibrium diffusion time for the shorter chain is smaller (Fig. 4c).

4.2. Healing strength and healing equilibrium time

Once we understand the inter-penetration behaviors of the polymer chains, we now study the self-healing behaviors of the nanocomposite hydrogels. For an original hydrogel sample, as the nominal stress gradually increases with the stretch (Fig. 5a), the polymer chains are gradually detached from the nanoparticles (Fig. 2c). Once most of the polymer chains are detached, the nominal stress begins to decrease. At the critical point (denoted by the red cross on the blue line in Fig. 5a), the hydrogel sample breaks into two parts, and the red cross indicates the tensile strength of the hydrogel s_1^m.

To explain the tensile strength of a hydrogel sample with a self-healed interface, we first plot the theoretical nominal stress of the self-healed region (green dash line in Fig. 5c using Eq. (28)) and capture the critical point with stretch λ_{1h}^m and tensile strength s_{1h}^m. According to Eqs. (29) and (24), we project the tensile strength s_{1h}^m onto the original stress-stretch curve (blue line) to obtain the critical stretch of the self-healed sample λ_{1h}^c. It means that the stress-stretch curve of the self-healed sample superposes the one of the original sample (shown as green dash line in Fig. 5b) until breaking at stretch λ_{1h}^c with tensile strength s_{1h}^m ($s_{1h}^m \le s_1^h$). This argument resolves the confusion in the self-healing polymer field: why the self-healed polymer features a stress-strain curve that superposes the one of the original polymer (Blaiszik et al., 2010; Burattini et al., 2010; Wojtecki et al., 2011; Wool, 2008; Wu et al., 2008; Yang and Urban, 2013). The reason for the superposition phenomena is that the self-healed region is so small that the stretch of the self-healed sample is approximately equal to the one of the virgin sample (shown as Eq. (24)), but the strength is determined by the self-healed region.

With increasing healing time t, the strength of the healed hydrogel sample increases accordingly (Fig. 5c). Here we define a term called *healing strength ratio* as

$$\rho = \frac{s_{1h}^m}{s_1^m} \tag{30}$$

We plot a characteristic healing strength ratio ρ in a function of healing time t in Fig. 5c. We find that the relationship between the healing strength ratio and the healing time follows an error-function-like form: the healing strength ratio ρ is

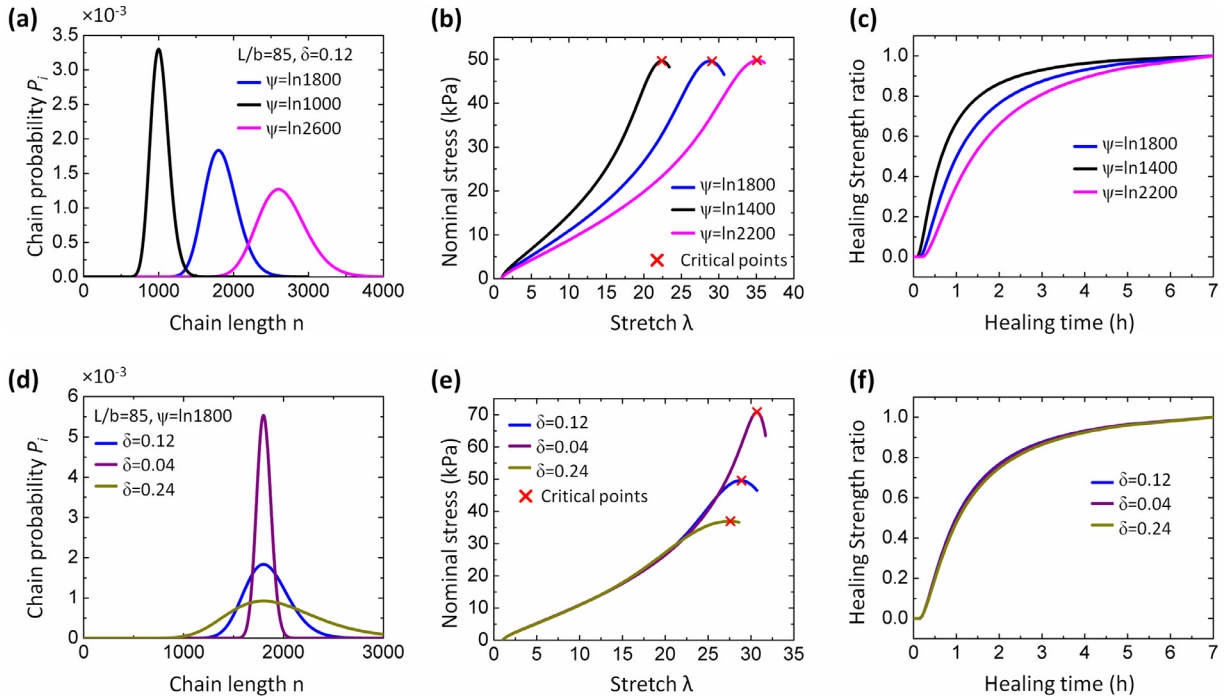

Fig. 6. Chain length distributions (a, d), stress-stretch behaviors of the original nanocomposite hydrogels (b, e) and the healing strength ratio versus healing time behaviors (c, f) for various average chain lengths ψ (a–c) and chain distribution widths δ (d–f). The following parameters are used to plot these curves: $\xi = 2.5 \times 10^{-8}$N/m and $\eta_p = 8.2 \times 10^{19}$m^{-3}.

initially nearly zero for small healing time and then increases monotonically within a transition region until approaching a plateau when the healing time is long enough. We further define a term called *equilibrium healing time* t_{eq} as the healing time when healing strength ratio ρ is equal to 0.9. This term indicates that after t_{eq} the strength of the healed sample is almost fully recovered with only 10% error. It is noted that equilibrium healing time t_{eq} is not equal to the equilibrium diffusion time t_e as discussed in Section 4.1, because t_e is chain-length dependent, but t_{eq} represents an effective behavior for all polymer chains.

4.3. Effects of model parameters on the healing behaviors

A number of model parameters affect the healing strength-time curve. Here we examine effects of chain length distribution, particle pair distance and Rouse friction coefficient.

4.3.1. Effect of chain length distribution

In this paper, we assume that the chain length distribution follows a log-normal form as shown in Eq. (2). The log-normal distribution is determined by two parameters: ψ indicating the average logarithm of the chain length and δ indicating the chain length distribution width. In Fig. 6, we maintain other material parameters and vary ψ and δ to examine their effects. First, with increasing ψ and constant δ, the average chain length increases accordingly (Fig. 6a); and the nanocomposite hydrogel can thus be stretched to a larger critical stretch until breaking (Fig. 6b). According to Eq. (15), longer chain length leads to smaller curvilinear diffusivity D_c of the polymer chains; therefore, the polymer chains need longer time to reach the nanoparticles and equilibrium healing time is longer (Fig. 6c). Second, with increasing δ and constant ψ, the chain distribution width increases with unchanged average chain length, and the chain probability for the average chain length is lower (Fig. 6d). The sharper (narrower) chain length distribution is corresponding to sharper stress behavior with higher maximum strength. However, due to the unchanged average chain length, the maximum stretchability of the nanocomposite hydrogel is almost unchanged (Fig. 6e). At the same time, the equilibrium healing time is almost unchanged (Fig. 6f). It does not mean that the chain length distribution width is not important for the self-healing model because different chain length distribution widths δ are corresponding to different stress-stretch behaviors and an appropriate δ is necessary for matching the stress-stretch behaviors of the nanocomposite hydrogels.

4.3.2. Effect of particle distance

With unchanged chain length distribution, we examine the effect of the particle distance L on the stress-stretch and self-healing behaviors shown in Fig. 7. The particle distance L affects the stress-stretch behaviors from two aspects: First, the

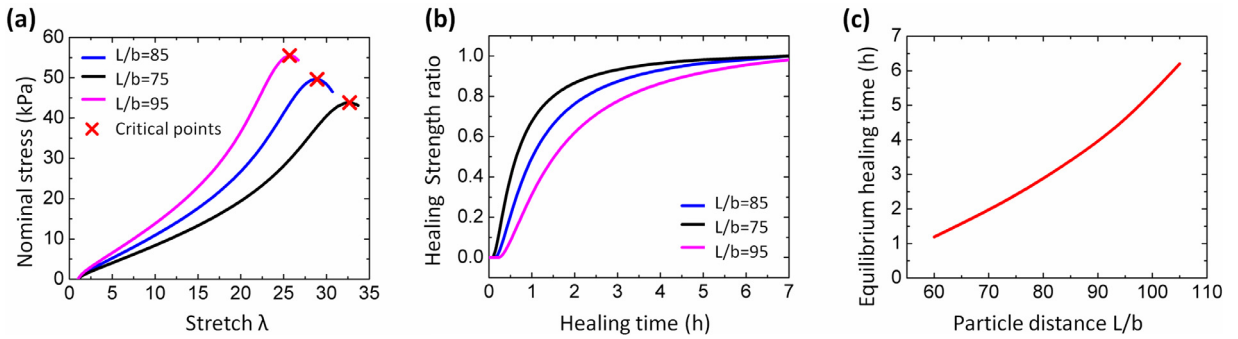

Fig. 7. (a) Stress-stretch behaviors of original nanocomposite hydrogels, (b) the healing strength ratio versus healing time behaviors and (c) equilibrium healing time for various particle distance. The following parameters are used to plot these curves: $\psi = \ln 1800$, $\delta = 0.12$, $\xi = 2.5 \times 10^{-8}$N/m, and $\eta_p = 8.2 \times 10^{19}$m^{-3}.

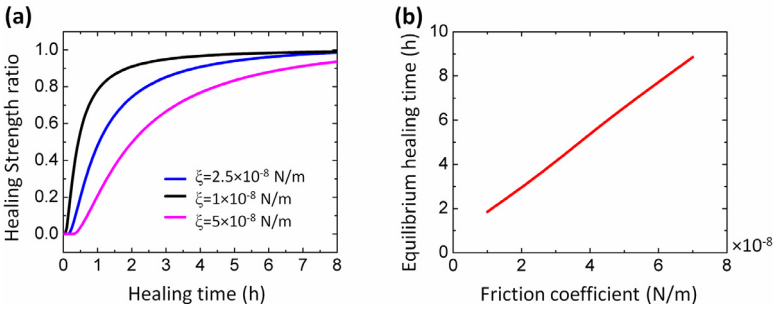

Fig. 8. (a) The healing strength ratio versus healing time behaviors and (b) equilibrium healing time for various Rouse friction coefficients. The following parameters are used to plot these curves: $L/b = 85$, $\psi = \ln\lfloor L^2/(4b^2)\rfloor$, $\delta = 0.12$, and $\eta_p = 8.2 \times 10^{19}$m^{-3}.

particle distance L is directly involved in the expression of the nominal stress of the nanocomposite hydrogel shown in Eq. (14); therefore, higher particle distance is corresponding to higher nominal stress with the same stretch (Fig. 7a). Second, the particle distance is also involved in the expression of the chain stretch of the ith chain shown in Eq. (6), which can be rewritten as

$$I_1 = \frac{3n_i\Lambda_i^2 b^2}{L^2} \tag{31}$$

According to Eq. (31), corresponding to the same chain stretch Λ_i, the larger particle distance L leads to lower overall hydrogel stretch; therefore, the overall stretchability of the nanocomposite hydrogel with larger particle distance is smaller (Fig. 7a). In addition, larger particle distance requires the polymer chains with free end groups to diffuse for a longer time to reach the other particle (shown in Fig. 3); therefore, the equilibrium healing time of the nanocomposite hydrogel sample increase with the increasing particle distance (Fig. 7bc).

4.3.3. Effect of Rouse friction coefficient

With unchanged chain length distribution and particle distance, we further vary the Rouse friction coefficient ξ in Fig. 8. As shown in Eq. (15), the curvilinear diffusion coefficient D_c of the polymer chains is in a reciprocal relationship with the Rouse friction coefficient. The higher friction coefficient leads to smaller chain diffusivity. Therefore, the polymer chains require longer time to diffuse within the nanocomposite hydrogel matrix and the corresponding equilibrium self-healing time should be longer (Fig. 8a, b). In addition, according to Eq. (15) and Fig. 3, the effective diffusion time of the ith chain across the nanocomposite hydrogel matrix to reach the other particle can be approximated as

$$t_i \sim \frac{L^4 n_i \xi}{16 b^2 k_B T} \tag{32}$$

Considering the correlationship between the diffusion time and the healing time, the equilibrium healing time t_{eq} should be approximately in a linear relationship with the friction coefficient. The theoretical result shown in Fig. 8b can also validate the linear relationship between the equilibrium healing time and the Rouse friction coefficient (Fig. 8b).

4.4. Comparison with self-healing experiments

After illustrating the effects of model parameters on the stress-stretch and healing behaviors of the nanocomposite hydrogels, we next validate these theoretical results with experimental data. We first use nanosilica particles (size ~9 nm) to

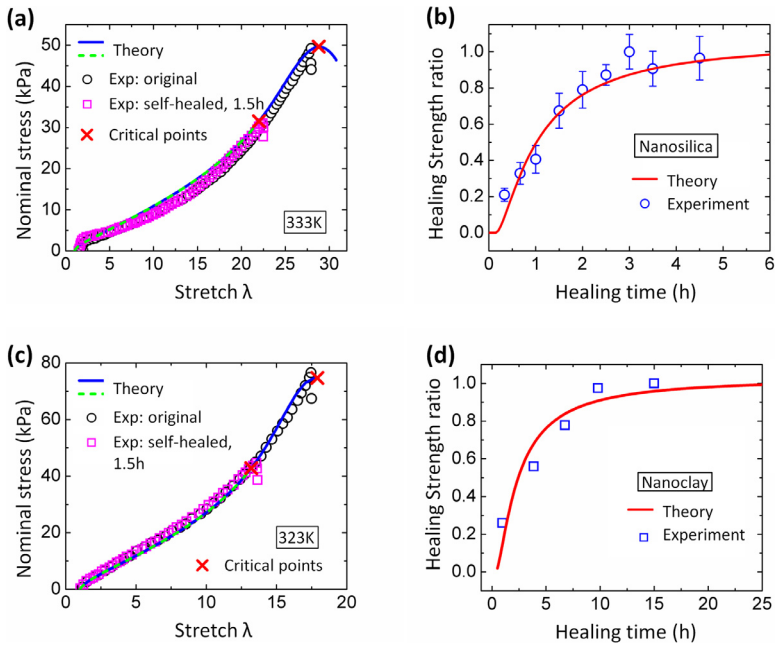

Fig. 9. Theoretically calculated and experimentally measured stress-stretch behaviors of the original and self-healing nanocomposite hydrogel samples (a, c), and healing strength ratio versus healing time behaviors (b, d) for nanosilica (a–b) and nanoclay crosslinkers (c–d). The parameters used to explain behaviors of nanosilica hydrogels: $L/b = 85$, $\psi = \ln(1806)$, $\delta = 0.12$, $\xi = 2.5 \times 10^{-8}$N/m, and $\eta_p = 8.2 \times 10^{19}$m^{-3}. The parameters used to explain behaviors of nanoclay hydrogels: $L/b = 50$, $\psi = \ln(625)$, $\delta = 0.12$, $\xi = 2 \times 10^{-6}$N/m, and $\eta_p = 3.24 \times 10^{22}$m^{-3}. The experimental results in (c) and (d) are from reference (Haraguchi et al., 2011).

crosslink N,N-Dimethylacrylamide chains to form nanocomposite hydrogels, and measure their stress-stretch behaviors (See Experimental section for details). As shown in Fig. 9a, our theory can accurately explain the stress-stretch behavior and tensile strength of the as-fabricated nanocomposite hydrogel with nanosilicas as the particle crosslinkers (Carlsson et al., 2010). Then, we cut the nanocomposite hydrogels into two parts, immediately bring them into contact with the breaking surfaces, and measure their stress-stretch behaviors after various healing time. As an example shown in Fig. 9a, our theoretical results can consistently match the measured stress-strain curve and the tensile strength of the healed sample with healing-time 1.5 h at 333 K. We further plot the theoretical healing strength ratio in a function of healing time in Fig. 9b. The theoretical results can also quantitatively match with our experimental results of the nanosilica hydrogels (Fig. 9b).

Not only by our experimental results of nanosilica hydrogels, can the theory also be validated by reported data on a nanocomposite hydrogel with nanoclay crosslinkers (Fig. 9c, d) (Haraguchi et al., 2011). In our recent paper (Wang and Gao, 2016), we showed that our theory with inhomogeneous chain length distribution can accurately capture the stress-stretch behaviors of the nanoclay hydrogels reported by Haraguchi *et al.* (Haraguchi, 2011b; Haraguchi et al., 2006; Haraguchi et al., 2003; Haraguchi and Li, 2006; Haraguchi and Takehisa, 2002; Haraguchi et al., 2011); here we further show that our self-healing theory can also capture the stress-stretch behaviors of the self-healed nanoclay hydrogels and corresponding healing strengths (Fig. 9cd).

It is noted that the material parameters in this paper include the following six: the nanoparticle volume concentration η_p, normalized particle-pair distance L/b, chain length distribution parameters ψ and δ, maximum chain-particle bonding strength f_{str}, and Rouse friction coefficient per Kuhn segment ξ. η_p is calculated using the material composition in the experiment. L/b, ψ, δ and f_{str} are obtained by fitting the stress-strain curves of the original nanocomposite hydrogels with the constitutive model in section 3.1 (Fig. 9ac). Rouse friction coefficient per Kuhn segment ξ is the only fitting parameter used to capture the self-healing behaviors. The used friction coefficients ξ in Fig. 9 are within the reasonable order compared with the experimental results in the references (Chapman et al., 1998; Whitlow and Wool, 1991).

4.5. Effect of healing temperature

To further demonstrate the capability of the theory, we examine effects of temperatures on the healing behaviors of the nanocomposite hydrogels. Due to the existence of water molecules within the hydrogel matrix, we only constrain the temperature range within 25°C-100 °C (298K-373 K). The experimental results in Fig. 10a show that the healing process of the nanosilica can be significantly accelerated by the higher temperature. The equilibrium healing time for the nanosilica hydrogels at 316 K is around 5 h, while only around 1 h at 353 K.

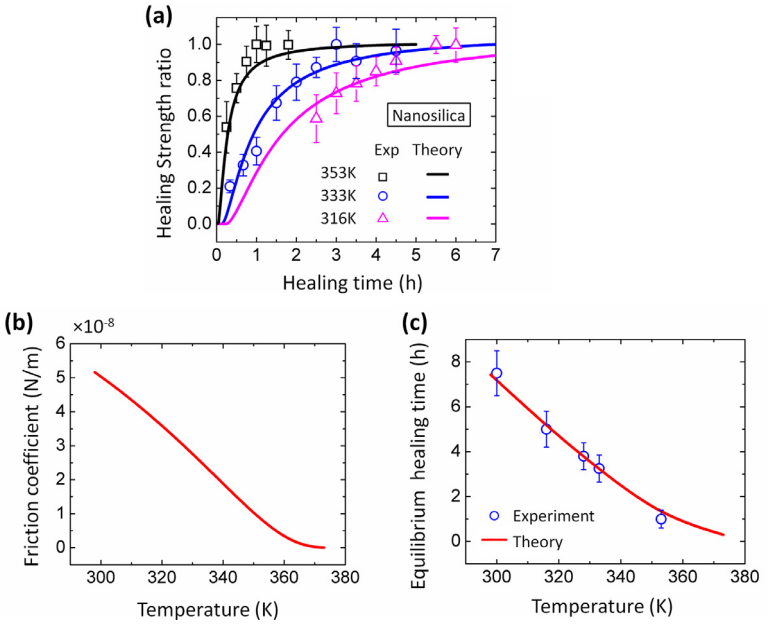

Fig. 10. Effects of temperatures on the self-healing behaviors of nanosilica hydrogels. (a) Theoretically calculated and experimentally measured healing strength ratios of the self-healed nanosilica hydrogels in functions of healing time at various healing temperatures. (b) Rouse friction coefficients in a function of healing temperature. (c) Theoretically calculated and experimentally measured equilibrium healing time in functions of healing temperatures. The parameters used to explain behaviors of nanosilica hydrogels: $L/b = 85$, $\psi = \ln(1806)$, $\delta = 0.12$, and $\eta_p = 8.2 \times 10^{19}\mathrm{m}^{-3}$.

The temperature term is directly involved in the expression of the nominal stress of the original hydrogel and self-healed hydrogel shown in Eqs. (14) and (28). However, the existence in both expressions results in the vanishing of temperature term in the healing strength ratio ρ. Here, we more focus on the effects of temperatures on the diffusion coefficient D_c (Eq. (15)). The curvilinear diffusivity can be affected by the temperature from two aspects: First, the temperature term explicitly appears in Eq. (15) through k_BT. In addition, the Rouse friction coefficient ξ monotonically decreases with increasing temperature(Rubinstein and Colby, 2003). This behavior can usually be modeled by Vogel relationship as (Rubinstein and Colby, 2003; Whitlow and Wool, 1991; Wool, 2008),

$$\xi \propto \exp\left(\frac{B}{T - T_\infty} - A\right) \tag{33}$$

where T_∞ is the Vogel temperature, B and A are constant parameters. Using parameters A = 15.71, B = 92 K and $T_\infty = 384.41$ K, we show that the Rouse friction coefficient monotonically decreases with increasing temperature shown in Fig. 10b. In turn, the friction coefficients can be used to explain the relationship between the healing strength ratio and healing time shown in Fig. 10a. The theoretical healing strength ratios consistently match the experimentally measured results. Further experiments show that the theoretical equilibrium healing time is in a good agreement with the measured results from 300 K to ~360 K (Fig. 10c).

Moreover, the Vogel relationship shown in Eq. (33) can also be used to explain the healing behaviors of the nanoclay hydrogels at various temperatures (Fig. 11). With parameters A = 31.81, B = 2149.9 K and $T_\infty = 206.14$ K, the theoretical healing strength ratio and equilibrium healing time can consistently match with the reported results of the nanoclay hydrogels from 310 K to 353 K (Haraguchi et al., 2011). We also notice that the Rouse friction coefficients of the nanoclay hydrogel are larger than those of the nanosilica hydrogels, which is highly probably due to the shape difference between the nanoclays and nanosilicas. Although it may be an interesting problem to elucidate the detailed mechanism how the hydrogel matrix configuration and particle geometry affect the Rouse friction coefficients, it may be out of the scope of the current paper.

4.6. Effect of particle concentration

Besides the temperature, we also experimentally observed that the equilibrium healing time of nanocomposite hydrogels increases with the nanoparticle concentrations (Fig. 12a) (Haraguchi et al., 2011). With increasing particle concentrations, the motions of the polymer chains are significantly constrained due to the decreasing free volumes within the hydrogels. We denote f as the free volume fraction of the hydrogel and the Rouse friction coefficient follows Doolittle scaling law as (Ferry, 1980; Rubinstein and Colby, 2003),

$$\xi \sim \exp(1/f) \tag{34}$$

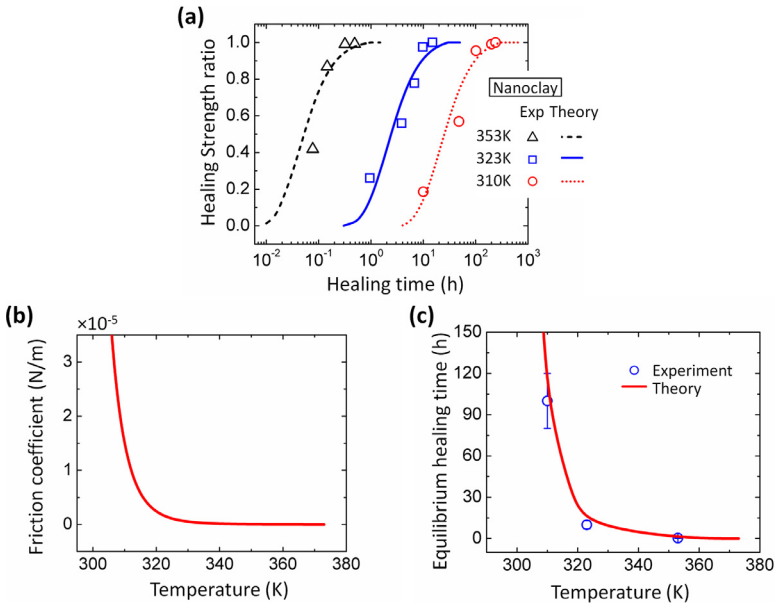

Fig. 11. Effects of temperatures on the self-healing behaviors of nanoclay hydrogels. (a) Theoretically calculated and experimentally measured healing strength ratios of the self-healed nanosilica hydrogels in functions of healing time at various healing temperatures. (b) Rouse friction coefficients in a function of healing temperatures. (c) Theoretically calculated and experimentally measured equilibrium healing time in functions of healing temperatures. The experimental results are from reference (Haraguchi et al., 2011). The parameters used to explain behaviors of nanoclay hydrogels: $L/b = 50$, $\psi = \ln(625)$, $\delta = 0.12$, and $\eta_p = 3.24 \times 10^{22}\mathrm{m}^{-3}$.

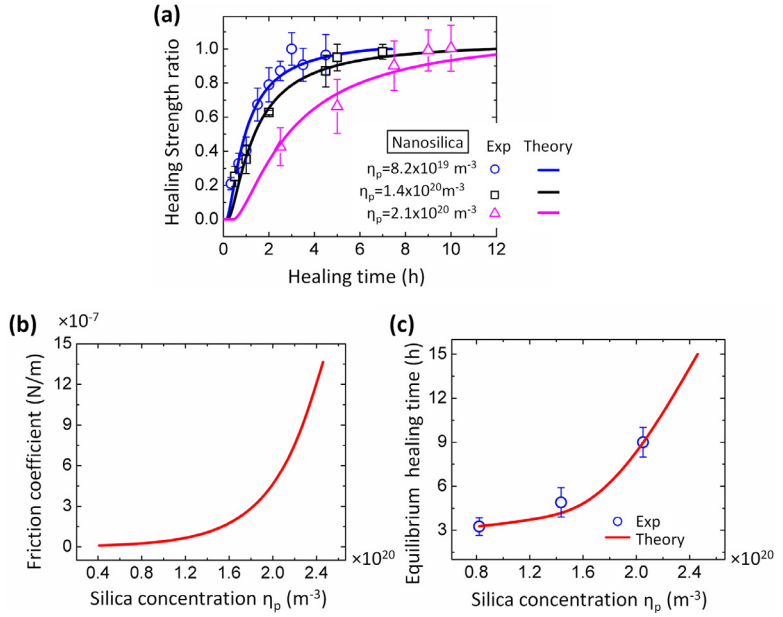

Fig. 12. Effects of nanosilica concentrations on the self-healing behaviors of nanosilica hydrogels. (a) Theoretically calculated and experimentally measured healing strength ratios of the self-healed nanosilica hydrogels with various nanosilica concentrations in functions of healing time. (b) Rouse friction coefficients in a function of healing temperature. (c) Theoretically calculated and experimentally measured equilibrium healing time in functions of nanosilica concentrations. The parameters used to explain behaviors of nanosilica hydrogels: $L/b = 85$, $\psi = \ln(1806)$, and $\delta = 0.12$.

With increasing nanoparticle concentration, the distance of the particles decreases and the free volume in the hydrogel thus decreases. We approximate the free volume fraction as

$$f \sim 1 - \eta_p v_0 \sim (1 + \eta_p v_0)^{-1} \tag{35}$$

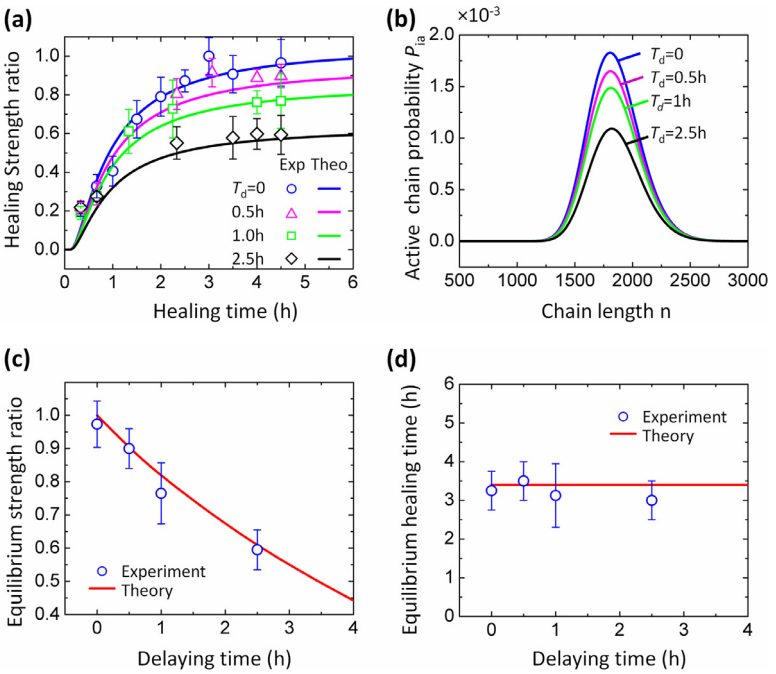

Fig. 13. Effects of delaying time on the self-healing behaviors of nanosilica hydrogels. (a) Theoretically calculated and experimentally measured healing strength ratios of the nanosilica hydrogels in functions of healing time for various delaying time. (b) The chain length distribution of the active chains for various delaying time. (c–d) Theoretically calculated and experimentally measured equilibrium strength ratios (c) and equilibrium healing time (d) in functions of the delaying time. The parameters used to explain behaviors of nanosilica hydrogels: $L/b = 85$, $\psi = \ln(1806)$, $\delta = 0.12$, $\xi = 2.5 \times 10^{-8}$N/m, and $\eta_p = 8.2 \times 10^{19}\mathrm{m}^{-3}$.

where ν_0 is the nanoparticle volume and $\eta_p \nu_0 << 1$ ($\nu_0 \sim 2.15 \times 10^{-25}$ m^3 for a 9 nm particle and $\eta_p \sim 10^{19}$-10^{23} m^{-3}). Therefore, we relate the Rouse friction coefficient to the particle concentration as

$$\xi \sim \exp(\eta_p \nu_0) \tag{36}$$

We first take the calculated ξ of a nanoclay hydrogel sample with $\eta_p = 8.2 \times 10^{19}\mathrm{m}^{-3}$ at 333 K to calculate the Rouse friction coefficient for various particle concentrations as shown in Fig. 12b. We then use the friction coefficients to calculate the healing strength ratios and the equilibrium healing time for various nanosilica concentrations (Fig. 12ac). As shown in Fig. 12ac, the theoretical healing strength and equilibrium healing time can consistently match with the experimentally measured results for nanosilica hydrogels with particle concentrations from $8.2 \times 10^{19}\mathrm{m}^{-3}$ to $2.1 \times 10^{20}\mathrm{m}^{-3}$.

4.7. Effect of delaying time

In the above theoretical modeling, we consider the healing process as immediately bringing two separated hydrogel parts into contact and heal. However, in the real applications and experiments, fractured self-healing materials usually undergo a delaying time t_d and then contact to heal. As revealed in the experiments (Fig. 13a), the maximum healing strength decreases with increasing delaying time t_d. It means the healing performance is degraded after a certain period of delaying. We can understand this behavior as follows.

During this delaying time, the polymer chains with free end groups initially on the hydrogel surfaces may degrade by diffusing into the matrix, or becoming inactive when encountering other molecular species. The degradation/dissipation behavior is complicated, mainly governed by the Rouse motion of the polymer chains (Rubinstein and Colby, 2003). To model the overall degradation of the chain free end groups, we consider an effective dissipation behavior following an exponential function with the delaying time t_d as (Rubinstein and Colby, 2003)

$$P_{ia} = \frac{N_{ia}}{N_i} \sim \exp\left(-\varphi \frac{t_d}{\tau_i}\right) \tag{37}$$

where $N_{ia}$is the available ith chain number after delaying time t_d, $P_{ia}$is the available ith chain probability on the hydrogel surface after delaying time t_d, φ is a constant and τ_i is the dissipation time scale for the ith chain. The dissipation time scale is mainly governed by the Rouse diffusion of the chain; therefore, τ_i can be written as

$$\tau_i = \frac{\xi}{k_B T} R^2 = \frac{\xi}{k_B T} n_i b^2 \tag{38}$$

where R is the characteristic length scale which can be approximated as the length of freely joint ith chain $\sqrt{n_i}b$.

Using Eqs. (37)–(38) with $\varphi = 7 \times 10^4$, we can plot the active chain probability P_{ia} as shown in Fig. 13b and calculate the healing strength ratio for various delaying time in Fig. 13a. The theoretical healing strength ratios match consistently with the experimentally measured results for delaying time from 0 to 2.5 h (Fig. 13a). Due to the chain degradation/dissipation, the equilibrium healing strength monotonically decreases with the increasing delaying time, also in a good agreement with the experiments (Fig. 13c). It is further noted that due to unchanged average chain length (shown in Fig. 13b), the equilibrium healing time of the nanocomposite hydrogels with varied delaying time remains unchanged (Fig. 13d). Therefore, the delayed self-healing only induces lower healing interfacial strength, but still requires a similar level of healing time to heal to the equilibrium strength.

5. Conclusive remarks

In summary, we report a mechanistic theory to explain the tensile strength of self-healing nanocomposite hydrogels with varied healing time. Our theory can reveal the effects of temperature, nanoparticle concentrations and delaying time on the healing behaviors, consistent with the experimental results on both nanosilica hydrogels and nanoclay hydrogels. To the best of our knowledge, this is the first analytical model to explain the tensile strength of self-healing hydrogels with dynamic bonds (Balazs, 2007; Wool, 2008). This model can potentially be extended to explain various self-healing polymers with a variety of dynamic bonds (Blaiszik et al., 2010; Burattini et al., 2010; Wojtecki et al., 2011; Wool, 2008; Wu et al., 2008; Yang and Urban, 2013), including dynamic covalent bonds (Chen et al., 2002; Ghosh and Urban, 2009; Skene and Lehn, 2004) and physical bonds (Burnworth et al., 2011; Chen et al., 2012; Cordier et al., 2008; Gulyuz and Okay, 2014; Haraguchi et al., 2011; Holten-Andersen et al., 2011; Nakahata et al., 2011; Okay, 2015; Phadke et al., 2012; Sijbesma et al., 1997; Sun et al., 2012; Sun et al., 2013; Wang et al., 2013; Wang et al., 2010).

Despite the great potential, we have to admit that the current theory is highly simplified in multiple aspects that require more careful consideration in the future studies. First, the chain-particle interaction is highly simplified by assuming that once the polymer chain free-end groups arrive at the nanoparticles they are immediately absorbed by the nanoparticles. This assumption is only valid for relatively strong chain-particle interactions with interaction time scale much shorter than the chain diffusion time scale; however, the problem may involve another time scale if the interaction time scale is comparable to the diffusion time scale (Hui and Long, 2012; Long et al., 2014).

Second, we here have not considered the instantaneous surface adhesion between two separated hydrogel parts. This limitation can be used to explain why the experimentally measured instantaneous healing strength of the nanocomposite hydrogel is not close to zero, but always a positive number (Fig. 9b, d). We expect future models to consider this instantaneous adhesion effect to fully capture the healing strength behaviors from very small healing time to long healing time.

Third, we here only consider the interfacial healing strength as the indicator of the healing performance, because the measurement of the interfacial strength in experiments is relatively easy and most of the researchers in self-healing community use the interfacial strength in their experiments (Blaiszik et al., 2010; Burattini et al., 2010; Wojtecki et al., 2011; Wool, 2008; Wu et al., 2008; Yang and Urban, 2013). The interfacial healing strength is an effective indicator only when the fracture point is corresponding to the maximum stress. The nanocomposite hydrogels (e.g., nanosilica and nanoclay hydrogels) fall into this category (Haraguchi, 2007, 2011b; Wang and Gao, 2016). In addition, the results of interfacial strength are reliable when the sample number is large enough to eliminate the effects of small defects. In the experiments, we always use multiple samples (up to 10 samples for each case) to validate the accuracy of the measurement. On the other hand, interfacial fracture energy has been used to characterize the healing performance (Sun et al., 2012; Zhao, 2014). The measurement of the interfacial fracture energy is more difficult and has been less adopted by the researchers in the self-healing community. To understand the interfacial fracture energy, we have to consider two parts of energies during the fracture process $\Omega \approx \Omega_0 + \Omega_D$, where the intrinsic fracture energy Ω_0 due to the detaching or fracture of the crossover chains, and the dissipated elastic energy Ω_D due to the loading-unloading in the processing zone (Zhao, 2014). To capture the contribution of Ω_D, we should take into account the loading-unloading behaviors of the self-healing nanocomposite hydrogels, which recently have been modeled by our theory and validated with experiments (Wang and Gao, 2016). The current paper only focuses on the interfacial strength, leaving the detailed understanding of the interfacial fracture energy in the future studies.

Acknowledgment

The research was supported by NSF grant CMMI-1649093.

References

Arruda, E.M., Boyce, M.C., 1993. A three-dimensional constitutive model for the large stretch behavior of rubber elastic materials. J. Mech. Phys. Solids. 41, 389–412.
Balazs, A.C., 2007. Modeling self-healing materials. Mater. Today 10, 18–23.
Bell, G.I., 1978. Models for the specific adhesion of cells to cells. Science 200, 618–627.
Blaiszik, B., Kramer, S., Olugebefola, S., Moore, J.S., Sottos, N.R., White, S.R., 2010. Self-healing polymers and composites. Annu. Rev. Mater. Res. 40, 179–211.
Bueche, F., 1960. Molecular basis for the Mullins effect. J. Appl. Polym. Sci. 4, 107–114.
Burattini, S., Greenland, B.W., Chappell, D., Colquhoun, H.M., Hayes, W., 2010. Healable polymeric materials: a tutorial review. Chem. Soc. Rev. 39, 1973–1985.

Burnworth, M., Tang, L., Kumpfer, J.R., Duncan, A.J., Beyer, F.L., Fiore, G.L., Rowan, S.J., Weder, C., 2011. Optically healable supramolecular polymers. Nature 472, 334–337.
Carlsson, L., Rose, S., Hourdet, D., Marcellan, A., 2010. Nano-hybrid self-crosslinked PDMA/silica hydrogels. Soft Matter 6, 3619–3631.
Chapman, B.R., Hamersky, M.W., Milhaupt, J.M., Kostelecky, C., Lodge, T.P., von Meerwall, E.D., Smith, S.D., 1998. Structure and dynamics of disordered tetrablock copolymers: composition and temperature dependence of local friction. Macromolecules 31, 4562–4573.
Chen, X., Dam, M.A., Ono, K., Mal, A., Shen, H., Nutt, S.R., Sheran, K., Wudl, F., 2002. A thermally re-mendable cross-linked polymeric material. Science 295, 1698–1702.
Chen, Y., Kushner, A.M., Williams, G.A., Guan, Z., 2012. Multiphase design of autonomic self-healing thermoplastic elastomers. Nat. Chem. 4, 467–472.
Cordier, P., Tournilhac, F., Soulié-Ziakovic, C., Leibler, L., 2008. Self-healing and thermoreversible rubber from supramolecular assembly. Nature 451, 977–980.
Crank, J., 1979. The Mathematics of Diffusion. Oxford University Press.
De Gennes, P.-G., 1979. Scaling Concepts in Polymer Physics. Cornell University Press.
de Gennes, P.G., 1971. Reptation of a polymer chain in the presence of fixed obstacles. J. Chem. Phys. 55, 572–579.
Doi, M., Edwards, S.F., 1978. Dynamics of concentrated polymer systems. Part 1.-Brownian motion in the equilibrium state. J. Chem. Soc., Faraday Trans. 74, 1789–1801.
Erman, B., Mark, J.E., 1997. Structures and Properties of Rubberlike Networks. Oxford University Press, Oxford.
Ferry, J.D., 1980. Viscoelastic Properties of Polymers. John Wiley & Sons.
Flory, P.J., 1953. Principles of Polymer Chemistry. Cornell University Press, Ithaca.
Flory, P.J., Rehner Jr, J., 1943. Statistical mechanics of cross-linked polymer networks II. Swelling. The Journal of Chemical Physics 11, 521–526.
Ge, T., Robbins, M.O., Perahia, D., Grest, G.S., 2014. Healing of polymer interfaces: interfacial dynamics, entanglements, and strength. Phys. Rev. E 90, 012602.
Ghosh, B., Urban, M.W., 2009. Self-repairing oxetane-substituted chitosan polyurethane networks. Science 323, 1458–1460.
Govindjee, S., Simo, J., 1991. A micro-mechanically based continuum damage model for carbon black-filled rubbers incorporating Mullins' effect. J. Mech. Phys. Solids. 39, 87–112.
Gulyuz, U., Okay, O., 2014. Self-healing poly (acrylic acid) hydrogels with shape memory behavior of high mechanical strength. Macromolecules 47, 6889–6899.
Haraguchi, K., 2007. Nanocomposite hydrogels. Curr. Opin. Solid State Mater. Sci. 11, 47–54.
Haraguchi, K., 2011a. Stimuli-responsive nanocomposite gels. Colloid. Polym. Sci. 289, 455–473.
Haraguchi, K., 2011b. Synthesis and properties of soft nanocomposite materials with novel organic/inorganic network structures. Polym. J. 43, 223–241.
Haraguchi, K., Ebato, M., Takehisa, T., 2006. Polymer–clay nanocomposites exhibiting abnormal necking phenomena accompanied by extremely large reversible elongations and excellent transparency. Adv. Mater. 18, 2250–2254.
Haraguchi, K., Farnworth, R., Ohbayashi, A., Takehisa, T., 2003. Compositional effects on mechanical properties of nanocomposite hydrogels composed of poly (N, N-dimethylacrylamide) and clay. Macromolecules 36, 5732–5741.
Haraguchi, K., Li, H.-J., 2006. Mechanical properties and structure of polymer-clay nanocomposite gels with high clay content. Macromolecules 39, 1898–1905.
Haraguchi, K., Li, H.-J., Song, L., Murata, K., 2007. Tunable optical and swelling/deswelling properties associated with control of the coil-to-globule transition of poly (N-isopropylacrylamide) in polymer-clay nanocomposite gels. Macromolecules 40, 6973–6980.
Haraguchi, K., Li, H.J., 2005. Control of the coil-to-globule transition and ultrahigh mechanical properties of PNIPA in nanocomposite hydrogels. Angew. Chem. Int. Ed. 44, 6500–6504.
Haraguchi, K., Song, L., 2007. Microstructures formed in co-cross-linked networks and their relationships to the optical and mechanical properties of PNIPA/clay nanocomposite gels. Macromolecules 40, 5526–5536.
Haraguchi, K., Takehisa, T., 2002. Nanocomposite hydrogels: a unique organic-inorganic network structure with extraordinary mechanical, optical, and swelling/de-swelling properties. Adv. Mater. 14, 1120–1124.
Haraguchi, K., Takehisa, T., Fan, S., 2002. Effects of clay content on the properties of nanocomposite hydrogels composed of poly (N-isopropylacrylamide) and clay. Macromolecules 35, 10162–10171.
Haraguchi, K., Uyama, K., Tanimoto, H., 2011. Self-healing in nanocomposite hydrogels. Macromol. Rapid Commun. 32, 1253–1258.
Holten-Andersen, N., Harrington, M.J., Birkedal, H., Lee, B.P., Messersmith, P.B., Lee, K.Y.C., Waite, J.H., 2011. pH-induced metal-ligand cross-links inspired by mussel yield self-healing polymer networks with near-covalent elastic moduli. Proc. Natl. Acad. Sci. USA 108, 2651–2655.
Hong, W., Zhao, X., Zhou, J., Suo, Z., 2008. A theory of coupled diffusion and large deformation in polymeric gels. J. Mech. Phys. Solids. 56, 1779–1793.
Huang, T., Xu, H., Jiao, K., Zhu, L., Brown, H.R., Wang, H., 2007. A novel hydrogel with high mechanical strength: a macromolecular microsphere composite hydrogel. Adv. Mater. 19, 1622–1626.
Hui, C.-Y., Long, R., 2012. A constitutive model for the large deformation of a self-healing gel. Soft Matter 8, 8209–8216.
Kim, H., Lee, K.-J., Lee, H.H., 1996. Healing of fractured polymers by interdiffusion. Polymer 37, 4593–4597.
Kim, Y.H., Wool, R.P., 1983. A theory of healing at a polymer-polymer interface. Macromolecules 16, 1115–1120.
Kuhn, W., Grün, F., 1942. Beziehungen zwischen elastischen Konstanten und Dehnungsdoppelbrechung hochelastischer Stoffe. Kolloid Z. 101, 248–271.
Long, R., Mayumi, K., Creton, C., Narita, T., Hui, C.-Y., 2014. Time dependent behavior of a dual cross-link self-healing gel: theory and experiments. Macromolecules 47, 7243–7250.
Mayumi, K., Guo, J., Narita, T., Hui, C.Y., Creton, C., 2016. Fracture of dual crosslink gels with permanent and transient crosslinks. Extreme Mechanics Letters 6, 52–59.
Morton, M., 2012. Anionic Polymerization: Principles and Practice. Elsevier.
Nakahata, M., Takashima, Y., Yamaguchi, H., Harada, A., 2011. Redox-responsive self-healing materials formed from host–guest polymers. Nat. Comm. 2, 511.
Okay, O., 2015. Self-Healing Hydrogels Formed Via Hydrophobic Interactions, Supramolecular Polymer Networks And Gels. Springer, pp. 101–142.
Phadke, A., Zhang, C., Arman, B., Hsu, C.-C., Mashelkar, R.A., Lele, A.K., Tauber, M.J., Arya, G., Varghese, S., 2012. Rapid self-healing hydrogels. Proc. Natl. Acad. Sci. USA 109, 4383–4388.
Ren, H.-Y., Zhu, M., Haraguchi, K., 2011. Characteristic swelling–deswelling of polymer/clay nanocomposite gels. Macromolecules 44, 8516–8526.
Ribas-Arino, J., Marx, D., 2012. Covalent mechanochemistry: theoretical concepts and computational tools with applications to molecular nanomechanics. Chem. Rev. 112, 5412–5487.
Rose, S., Prevoteau, A., Elzière, P., Hourdet, D., Marcellan, A., Leibler, L., 2014. Nanoparticle solutions as adhesives for gels and biological tissues. Nature 505, 382–385.
Rouse Jr, P.E., 1953. A theory of the linear viscoelastic properties of dilute solutions of coiling polymers. J. Chem. Phys. 21, 1272–1280.
Rubinstein, M., Colby, R., 2003. Polymer Physics. Oxford University Press, Oxford.
Sijbesma, R.P., Beijer, F.H., Brunsveld, L., Folmer, B.J., Hirschberg, J.K., Lange, R.F., Lowe, J.K., Meijer, E., 1997. Reversible polymers formed from self-complementary monomers using quadruple hydrogen bonding. Science 278, 1601–1604.
Skene, W.G., Lehn, J.-M.P., 2004. Dynamers: polyacylhydrazone reversible covalent polymers, component exchange, and constitutional diversity. Proc. Natl. Acad. Sci. USA 101, 8270–8275.
Stukalin, E.B., Cai, L.-H., Kumar, N.A., Leibler, L., Rubinstein, M., 2013. Self-healing of unentangled polymer networks with reversible bonds. Macromolecules 46, 7525–7541.
Sun, J.-Y., Zhao, X., Illeperuma, W.R., Chaudhuri, O., Oh, K.H., Mooney, D.J., Vlassak, J.J., Suo, Z., 2012. Highly stretchable and tough hydrogels. Nature 489, 133–136.
Sun, T.L., Kurokawa, T., Kuroda, S., Ihsan, A.B., Akasaki, T., Sato, K., Haque, M.A., Nakajima, T., Gong, J.P., 2013. Physical hydrogels composed of polyampholytes demonstrate high toughness and viscoelasticity. Nat. Mater. 12, 932–937.

Toohey, K.S., Sottos, N.R., Lewis, J.A., Moore, J.S., White, S.R., 2007. Self-healing materials with microvascular networks. Nat. Mater. 6, 581–585.
Treloar, L.R.G., 1975. The Physics of Rubber Elasticity. Oxford University Press, Oxford.
Wang, C., Liu, N., Allen, R., Tok, J.B.H., Wu, Y., Zhang, F., Chen, Y., Bao, Z., 2013. A rapid and efficient self-healing thermo-reversible elastomer crosslinked with graphene oxide. Adv. Mater. 25, 5785–5790.
Wang, Q., Gao, Z., 2016. A constitutive model of nanocomposite hydrogels with nanoparticle crosslinkers. J. Mech. Phys. Solids. 94, 127–147.
Wang, Q., Gossweiler, G.R., Craig, S.L., Zhao, X., 2015. Mechanics of mechanochemically responsive elastomers. J. Mech. Phys. Solids. 82, 320–344.
Wang, Q., Mynar, J.L., Yoshida, M., Lee, E., Lee, M., Okuro, K., Kinbara, K., Aida, T., 2010. High-water-content mouldable hydrogels by mixing clay and a dendritic molecular binder. Nature 463, 339–343.
White, S.R., Sottos, N., Geubelle, P., Moore, J., Kessler, M.R., Sriram, S., Brown, E., Viswanathan, S., 2001. Autonomic healing of polymer composites. Nature 409, 794–797.
Whitlow, S.J., Wool, R.P., 1991. Diffusion of polymers at interfaces: a secondary ion mass spectroscopy study. Macromolecules 24, 5926–5938.
Williams, G.A., Ishige, R., Cromwell, O.R., Chung, J., Takahara, A., Guan, Z., 2015. Mechanically robust and self-healable superlattice nanocomposites by self-assembly of single-component “sticky” polymer-grafted nanoparticles. Adv. Mater. 27, 3934–3941.
Wojtecki, R.J., Meador, M.A., Rowan, S.J., 2011. Using the dynamic bond to access macroscopically responsive structurally dynamic polymers. Nat. Mater. 10, 14–27.
Wool, R., O’connor, K., 1981. A theory crack healing in polymers. J. Appl. Phys. 52, 5953–5963.
Wool, R.P., 1995. Polymer Interfaces: Structure and Strength. Hanser.
Wool, R.P., 2008. Self-healing materials: a review. Soft Matter 4, 400–418.
Wu, D.Y., Meure, S., Solomon, D., 2008. Self-healing polymeric materials: a review of recent developments. Prog. Polym. Sci. 33, 479–522.
Yang, Y., Urban, M.W., 2013. Self-healing polymeric materials. Chem. Soc. Rev. 42, 7446–7467.
Yu, K., Shi, Q., Li, H., Jabour, J., Yang, H., Dunn, M.L., Wang, T., Qi, H.J., 2016. Interfacial welding of dynamic covalent network polymers. J. Mech. Phys. Solids. 94, 1–17.
Zhang, H., Wool, R.P., 1989. Concentration profile for a polymer-polymer interface. 1. Identical chemical composition and molecular weight. Macromolecules 22, 3018–3021.
Zhang, M.Q., Rong, M.Z., 2012. Theoretical consideration and modeling of self-healing polymers. J. Polymer Sci. Part B 50, 229–241.
Zhao, X., 2014. Multi-scale multi-mechanism design of tough hydrogels: building dissipation into stretchy networks. Soft Matter 10, 672–687.